Framework mobility in the metal–organic framework crystal IRMOF-3: Evidence for aromatic ring and amine rotation

William Morris [a], R.E. Taylor [a,*], C. Dybowski [b], Omar M. Yaghi [a], Miguel A. Garcia-Garibay [a,*]

[a] Department of Chemistry and Biochemistry, University of California, Los Angeles, Los Angeles, CA 90095-1569, USA
[b] Department of Chemistry and Biochemistry, University of Delaware, Newark, DE 19716-2522, USA

ABSTRACT

The framework motions in IRMOF-3 ($Zn_4O(BDC-NH_2)_3$), where BDC-NH_2 represents 2-amino-1,4-benzenedicarboxylate, have been investigated with ^1H NMR relaxation measurements. Isotopic enrichment of the 2-amino group with ^{15}N was critical in elucidating the lattice dynamics and enhancing spectral resolution. These results indicate a low energy process associated with rotation of the amino group, with an activation energy of 1.8 ± 0.6 kcal/mol, and full 180° rotation of the phenylene group in the BDC-NH_2 moiety with an activation energy of 5.0 ± 0.2 kcal/mol. A relatively low pre-exponential factor for amine rotation ($1.3 \times 10^7 \, s^{-1}$) is tentatively associated with the need to break a hydrogen bond as the rate-limiting step. Both amine rotation and the aromatic ring flip occur at frequencies that provide an effective relaxation mechanism for the 99.6% natural abundance quadrupolar ^{14}N in the amino group. Dipolar coupling of the ^{14}N to adjacent spin-½ nuclei (both ^1H and ^{13}C) occurs not only in the static sample but also in the MAS experiments at the 7 T magnetic field used in this study. As a result, the spin dynamics and the cross-polarization dynamics are affected, resulting in spectral broadening. In the MAS experiments, isotopic replacement of the natural abundance ^{14}N with ^{15}N significantly improves resolution of the ^{15}N spectra as well as in the ^1H and ^{13}C spectra.

© 2011 Elsevier B.V. All rights reserved.

1. Introduction

Metal organic frameworks (MOFs) are crystalline porous materials where porosity and functionality can be controlled on the nanoscale by choice of the metal secondary building unit (SBU) and the organic linker [1–3]. Such control is highlighted by the ability to synthesize isoreticular metal organic frameworks (IRMOFs) in which the topology of various structures is the same, but the functionality and surface area can be systematically changed by variation in the organic moiety [4–6]. Over 20 IRMOFs have been reported of the MOF-5 $Zn_4O(BDC)_3$ structure (where BDC represents 1,4-benzenedicarboxylate), with changes in surface area and functionality leading to potential applications in gas storage [7,8]. One such MOF, IRMOF-3 ($Zn_4O(BDC-NH_2)_3$) has been the focus of several studies due to the free amine functionality it possesses [9–12]. A 2-amino group on the 1,4-benzenedicarboxylate allows organic reactions to occur in the pores of MOF materials in what has been termed postmodification [13,14]. In addition, incorporation of amine groups has been shown to enhance CO_2 uptake in porous frameworks [15].

To realize the potential of these frameworks for gas-storage applications, lattice dynamics must be understood, as this affects guest molecule diffusion [16–19]. Furthermore, it has been suggested that control of internal dynamics may open opportunities for the development of functional materials and artificial molecular machines [20] and it has been shown that linker dynamics are responsible for the remarkable negative coefficient of thermal expansion of these interesting materials [21,22]. Although the overall MOF structure is rigidly arranged in an extended crystalline network, nuclear magnetic resonance (NMR) studies have shown that rotation of the BDC rings may occur. An activation energy of 11.3 kcal/mol has been derived for the ring-flipping motions in MOF-5 by ^2H NMR line-shape analyses [18], and dielectric measurements [19] of IRMOF-2 ($Zn_4O(BDC-Br)_3$) with a 2-bromo-1,4-benzenedicarboxylate indicate a rotational barrier of only 7.3 kcal/mol.

In this report, the dynamics of the amino-substituted IRMOF-3 ($Zn_4O(BDC-NH_2)_3$) have been investigated with ^1H NMR relaxation measurements. The structure has been characterized with ^{13}C and ^{15}N cross-polarization/magic-angle spinning (CP/MAS) [23] spectra.

2. Experimental

The synthesis and isotopic enrichment of IRMOF-3 are described below. All reagents, unless otherwise stated, were obtained

* Corresponding authors.
    E-mail addresses: taylor@chem.ucla.edu (R.E. Taylor), mgg@chem.ucla.edu (M.A. Garcia-Garibay).

from commercial sources (Alfa Aesar, Cambridge Isotope Laboratories, Sigma Aldrich, TCI) and were used without further purification. The reported yields reported were not optimized.

2.1. Synthesis of labeled compound

2.1.1. Diethyl 2-nitroterephthalate-^{15}N

Labeled ^{15}N potassium nitrate (1.191 g, 11.7 mmol) was added to nitromethane (10 mL) and stirred at room temperature. To the solution was added trifluoromethanesulfonic acid until the potassium nitrate was fully dissolved. Phosphorus pentoxide (3.43 g, 27.8 mmol) was added to the solution, followed by diethyl terephthalate acid (1.5 g, 6.8 mmol) in 10 mL of nitromethane. The solution was heated at 50 °C for 8 h. Upon cooling, water (50 mL) was slowly added to quench the unreacted phosphorus pentoxide. The solution was extracted with CH_3NO_2 (3 × 20 mL). The organic phase was removed under reduced pressure to yield diethyl 2-nitroterephthalate (1.3 g, 4.9 mmol, 72% yield).

2.1.2. Diethyl 2-aminoterephthalate-^{15}N

Diethyl 2-nitroterephthalate (1.3 g, 4.9 mmol) was dissolved in dry tetrahydrofuran (50 mL) and placed in a Parr high pressure reactor. To the solution was added Pd/charcoal (10% 0.1 g) and the reactor was sealed. The reaction was pressurized to five bar with hydrogen, and stirred for 24 h at room temperature. The reaction was filtered through Celite to remove the Pd/charcoal and washed with an excess of tetrahydrofuran. The organic phase was removed under reduced pressure to yield diethyl 2-aminoterephthalate (1.1 g, 4.6 mmol, yield 94%).

2.1.3. 2-Aminoterephthalic acid-^{15}N

Diethyl 2-aminoterephthalate (1.1 g 4.6 mmol) was dissolved in methanol (35 mL) and water (15 mL). Sodium hydroxide (1.84 g, 46 mmol) was added, and the resulting mixture was stirred at room temperature for 24 h. The MeOH/H$_2$O was removed under reduced pressure and the precipitate was redissolved in minimum water, and 2-aminoterephthalic acid was precipitated out of the solution by addition of excess HCl (1 M). The product was isolated by filtration and washed with water (5 × 50 mL) to yield a yellow solid (0.7 g, 3.8 mmol, yield 83%).

2.1.4. Synthesis of IRMOF-3

IRMOF-3 (Zn$_4$O(BDC-NH$_2$)$_3$) was synthesized using a literature procedure [24]. The ^{15}N-labeled IRMOF-3 was synthesized by an analogous preparation, replacing the natural abundance 2-aminoterephthalic acid (^{14}N natural abundance of 99.6% [25]) with the analogous 2-aminoterephthalic acid-^{15}N. Complete evacuation of the framework was confirmed by surface area measurements that showed surface areas of 2163 m^2/g (BET method) and 2120 m^2/g (BET method) measured for the natural abundance IRMOF-3 and isotopically enriched IRMOF-3, respectively. These surface areas correspond well with those reported previously [24]. A fragment of the extended structure of IRMOF-3 is shown in Fig. 1A.

The NMR data were acquired with a Bruker Avance 300 spectrometer. Proton data for static samples were measured with a standard Bruker ^{1}H wideline probe with a 5-mm solenoid coil. The ^{1}H π/2 pulse width was 1 μs. The ^{1}H spin–lattice relaxation (T_1) data were acquired with a saturation-recovery sequence [24] and the ^{1}H spin–lattice relaxation in the rotating frame ($T_{1\rho}$) was determined with a spin-locking sequence [26] ($\pi/2_x$ – (spin lock)$_y$) using a spin-locking field strength of 62.5 kHz.

High resolution solid-state ^{13}C and ^{15}N CP/MAS spectra were acquired with a magic-angle spinning (MAS) probe with a 4-mm (outside diameter) zirconia rotor. The acquisition parameters were a ^{1}H π/2 pulse width of 4 μs, a contact time of 3 ms, a data acquisition time of 65 ms, and a recycle delay of at least 5 times the ^{1}H
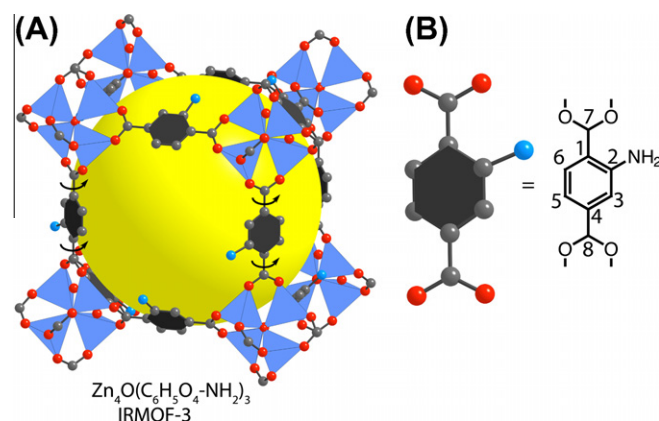

Fig. 1. The structure of IRMOF-3 (A). The sphere represents the free volume within the framework. The numerical labeling in (B) is used to note ^{13}C spectral assignments.

spin–lattice relaxation time, with recycle delays ranging from 5 to 30 s. The sample spinning rate was 10.000(±0.004) kHz. The ^{1}H combined rotation and multiple-pulse (CRAMPS) spectra [27] were acquired on the same 4-mm MAS probe with a ^{1}H π/2 pulse width of 2 μs and τ = 4 μs for the quadrature-detected BR-24 pulse sequence [28]. The sample spinning rate for the CRAMPS experiments was 3.000(±0.004) kHz. Performance of the CRAMPS experiment was checked with an α glycine standard.

The ^{13}C spectra are referenced to tetramethylsilane at zero ppm by use of the methylene resonance of adamantane at 37.77 ppm as a secondary reference [29]. The ^{15}N spectra are referenced to liquid ammonia at zero ppm by use of the ^{15}N resonance of α-glycine at 36.5 ppm as a secondary reference [25]. On this scale, nitromethane resonates at 382 ppm. The ^{1}H CRAMPS spectra are referenced to tetrakistrimethylsilylsilane at zero ppm.

3. Results and discussion

The ^{1}H wideline NMR spectrum of a polycrystalline, static sample of IRMOF-3 at 297 K is shown in Fig. 2A. The spectrum shows several features, rather than the broad structureless resonance usually observed for a typical polycrystalline solid sample. These result from the attenuation of the proton homonuclear dipolar coupling by the relatively rapid anisotropic motion. Lowering the sample temperature to 180 K does not slow this motion sufficiently to broaden the lineshape, as shown in Fig. 2B.

The ^{1}H spin–lattice relaxation behavior at 295 K is shown in Fig. 3, as determined with a saturation-recovery pulse sequence. The data are not strictly described by a single exponential function. Nonexponential recovery is often observed when paramagnetic centers, cross-relaxation, or spin diffusion plays a role in the relaxation kinetics [30–34]. For IRMOF-3, the ^{14}N of the amino substituent on the terephthalic acid linker provides an effective relaxation center (*vide infra*) for the protons [33]. The quadrupolar nucleus is effectively relaxed by movements of the aromatic ring near the quadrupolar frequency. Typical ^{14}N quadrupolar coupling constants are on the order of 1 MHz, depending upon the symmetry of the site. For example, the quadrupolar coupling constant (QCC) for choline halides [35] is about 70 kHz because of the relatively symmetric environment. For amino acids [36], the QCC is around 1.2 MHz; for formamide [37] it is 2.56 MHz; and for hydrazine [38], it is about 4 MHz. Aromatic ring π flips approaching, or at, this frequency provide an effective relaxation mechanism for the ^{14}N. The ^{14}N is both dipolar and scalar coupled to the amino protons, allowing the fast-relaxing quadrupolar nucleus to provide a

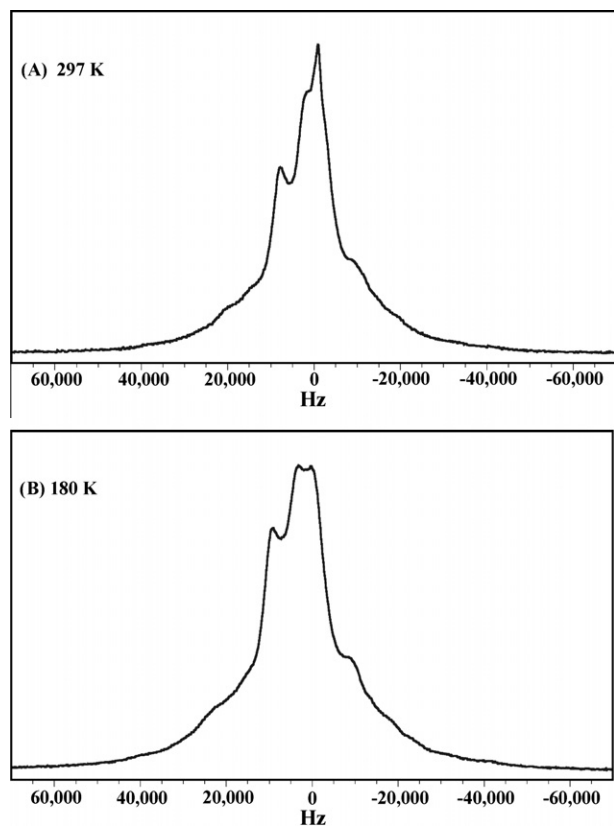**Fig. 2.** ^{1}H wide-line NMR spectra of IRMOF-3. The top spectrum (A) was acquired at 297 K, and the bottom (B) was acquired at 180 K.
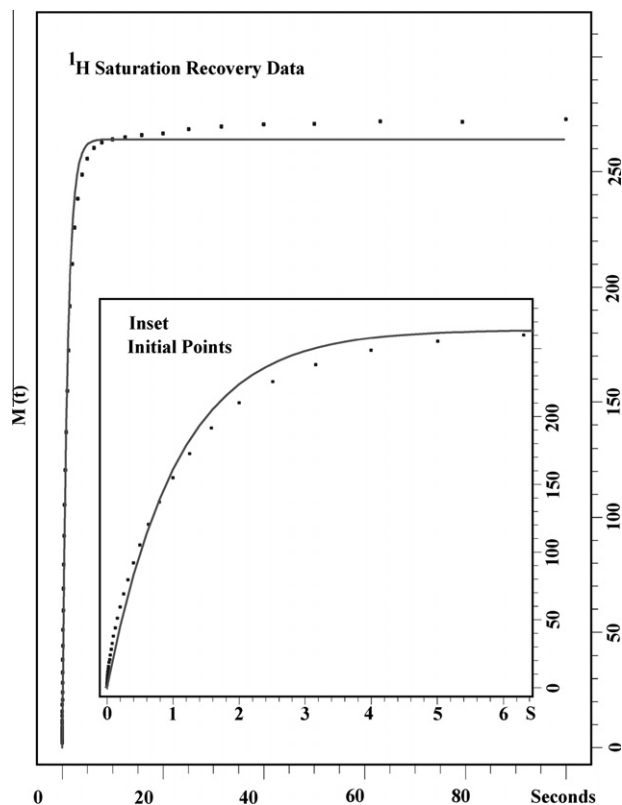

Fig. 3. [1]H saturation-recovery spin–lattice relaxation data for IRMOF-3 taken at a temperature of 295 K plotted in arbitrary units. The inset shows an expanded view of the initial data points. The smooth line in each is a fit to a single exponential recovery.

relaxation mechanism for these protons [33]. The amino protons are, in turn, dipolar coupled to the aromatic protons, which are effectively relaxed through spin diffusion mediated by these couplings. Although this mechanism accounts for the nonexponential behavior of the saturation-recovery data shown in Fig. 3, the time response can be reasonably approximated by an exponential function over a wide range of time. This approximation of the relaxation behavior is a sensitive barometer of the framework mobilities, allowing one to determine the corresponding activation parameters by monitoring changes in spin–lattice relaxation as a function of temperature (*vide infra*).

As a result of fast ^{14}N relaxation arising from the aromatic ring π flips, the ^{1}H spin–lattice relaxation values are relatively insensitive to temperature over the accessible temperature range for IRMOF-3 containing ^{14}N at natural abundance, as shown in Fig. 4 (square symbols). Although the proton saturation-recovery behavior is not strictly exponential, as indicated by the relatively small deviations shown in Fig. 3, the ^{1}H spin–lattice relaxation time constants, $T_{1approx}$, plotted in Fig. 4 are obtained by treating the saturation recovery data as approximately exponential in character.

This explanation of the sample's spin–lattice relaxation behavior is confirmed by data obtained from a sample of IRMOF-3 in which the ^{14}N is isotopically substituted with [15]N. In this highly ^{15}N-enriched sample, the ^{1}H saturation-recovery data also is nonexponential, but again can be reasonably approximated with a single exponential, as shown in Fig. 5. In contrast to the highly ^{15}N-enriched sample, the unlabeled material shows an additional strong relaxation contribution at low temperatures (Fig. 4, rhomboid symbols).

The isotopic substitution of ^{15}N for ^{14}N in IRMOF-3 also has a significant effect upon the ^{13}C, ^{15}N, and ^{1}H spectra. In particular, the MAS line widths are narrowed by the substitution of ^{15}N for
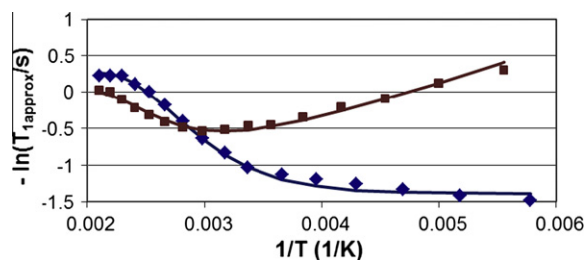
Fig. 4. The negative of the logarithm of the ^{1}H spin–lattice relaxation time ($T_{1approx}$) as a function of the inverse temperature for IRMOF-3 (♦ – enriched with ^{15}N; ■ – at natural abundance, 99.6% [14]N). The solid lines are simulations, as described in the text.

[14]N. This effect is shown for the ^{13}C CP/MAS spectra in Fig. 6. In the spectrum of the highly ^{15}N-enriched IRMOF-3 (Fig. 6B), the two carboxyl resonances are fully resolved. Of particular note is the increased intensity of the resonance of the ring carbon with the attached amino group at 149.7 ppm. The ring carbons with the attached carboxyl groups at 136.8 ppm and 115.4 ppm are also quite sharp, while the protonated ring carbons at 131.5 ppm, 117.8 ppm and the shoulder at 116.3 ppm are slightly broader with a lower intensity. The difference in the ^{13}C line widths results from molecular motion with the same timescale as the coherent averaging of the radiofrequency decoupling [39]. Spectral assignments of the aromatic ^{13}C resonances are based on additivity relationships [40].

At the relatively modest magnetic field of 7 T used in this study, the dipolar coupling of the quadrupolar ^{14}N to spin-½ nuclei is not averaged by magic-angle spinning [41–44]. At this magnetic field
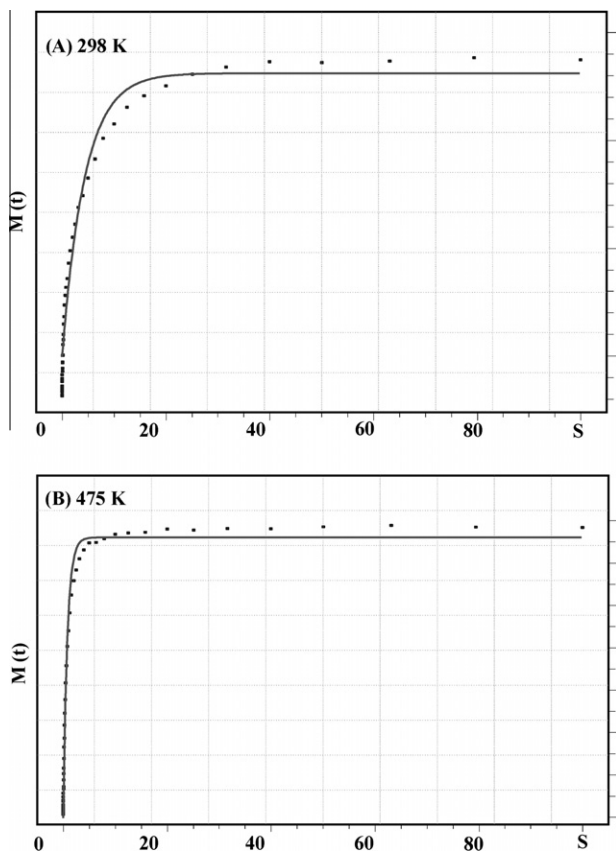
Fig. 5. ^{1}H saturation-recovery data for the ^{15}N-enriched IRMOF-3 at 298 K (A) and at 475 K (B) plotted in arbitrary units. The smooth line in each is a fit to a single-exponential recovery.

Fig. 6. ^{13}C CP/MAS spectra of a sample of IRMOF-3 containing ^{14}N at the natural abundance (A) and of a sample highly enriched in ^{15}N (B). The ^{13}C spectral assignments given by the numerals in (B) refer to the scheme given in Fig. 1B.

strength, the electric quadrupole interaction for the ^{14}N is comparable to the Zeeman interaction and results in a mixing of the pure Zeeman states. New terms in the resulting dipolar Hamiltonian are not averaged by magic-angle spinning. The isotopic replacement of ^{14}N with ^{15}N allows MAS to average this dipolar coupling, resulting in the observed narrowing.

A similar improved resolution can be seen in the ^{15}N CP/MAS spectra of IRMOF-3 in Fig. 7. The ^{15}N spectrum for the sample containing ^{14}N at the natural abundance of 99.6% (top spectrum) shows a broad resonance, as well as a low signal-to-noise ratio, in comparison to the highly ^{15}N-enriched sample (bottom spectrum). The very low signal-to-noise ratio of the ^{15}N spectrum of the natural-abundance sample arises from the fact that the IRMOFs are low-density materials, i.e., porous structures. Completely filling the MAS rotors with sample leads to a very small quantity of ^{15}N nuclei in the natural-abundance IRMOF-3 sample. The ^{15}N resonance at 60.5 ppm confirms the presence of the amino group, as the $-NH_3^+$ resonance is strongly deshielding, appearing at 139 ppm.

The same narrowing effects are observed in the ^{1}H CRAMPS spectra of ^{15}N-enriched IRMOF-3 in Fig. 8. This is additional evidence of the strong proton coupling to the ^{14}N in unlabeled samples. Deconvolution of the spectrum yields the expected 3:2 ratio for the aromatic protons to those of the amino group (not shown).

The narrowing of the resonances in the ^{1}H, ^{13}C, and ^{15}N spectra in the highly enriched ^{15}N sample suggests a difference in the cross-polarization dynamics between the two samples. This difference is clearly seen in the ^{13}C CP/MAS variable-contact-time data of the carboxyl resonances of the two samples, shown in Fig. 9. Similar behavior is also seen in Fig. 10 for the aromatic ring carbon
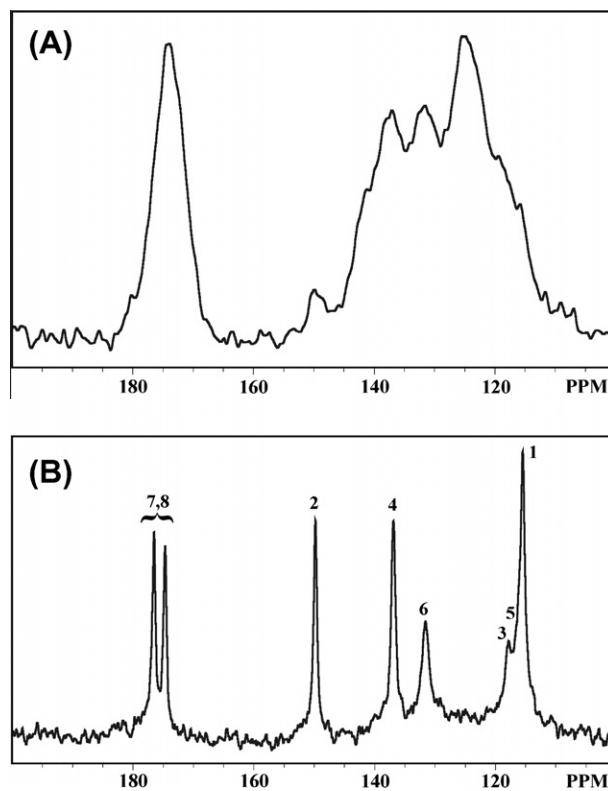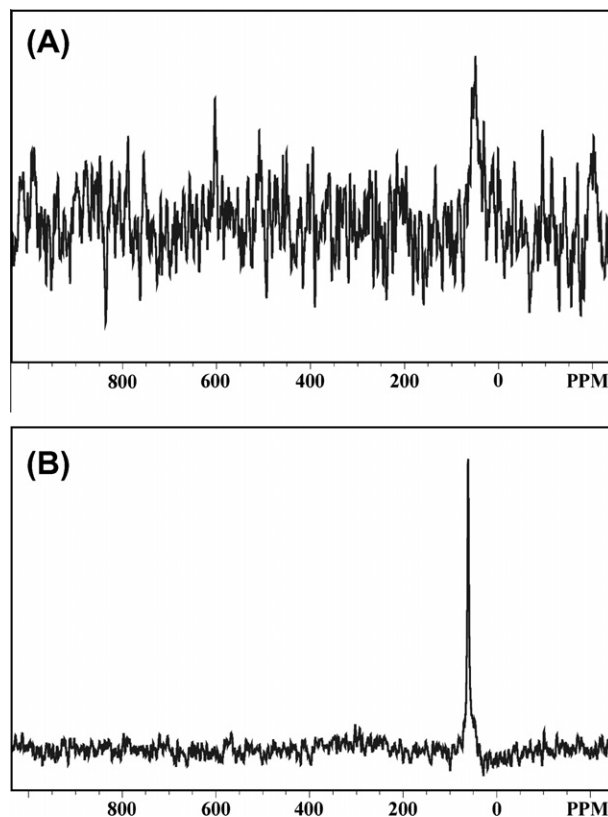

Fig. 7. ^{15}N CP/MAS spectra of a sample of IRMOF-3 containing ^{14}N at natural abundance (A) and of a sample highly enriched in ^{15}N (B).
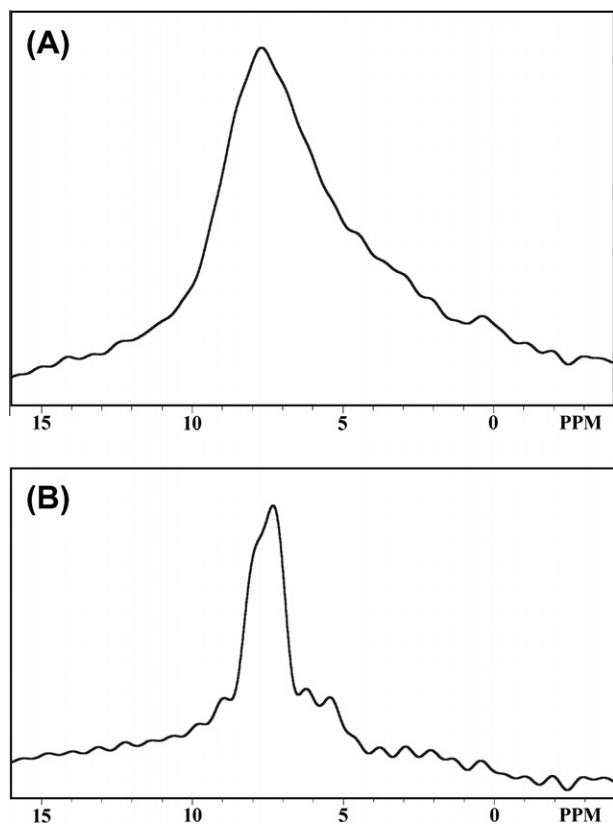
Fig. 8. [1]H CRAMPS spectra of a sample of IRMOF-3 containing ^{14}N at natural abundance (A) and of a sample highly enriched in [15]N (B).

substituted with the amino group. The smooth lines shown in Figs. 9 and 10 are fits of the theoretical expression from Mehring [45] to describe the polarization transfer behavior as a function of the contact time.

The recovery of the ^{1}H magnetization subject to a spin-lock field in the rotating frame ($T_{1\rho}$) at 297 K is shown in Fig. 11 over a time window of 20 ms. Again, the relaxation to equilibrium is nonexponential. The decay is well described by a biexponential function. However, rather than indicating the existence to two separate $T_{1\rho}$ processes affecting independent regions of the sample, the biexponentiality reflects the fact that the attenuated homonuclear dipolar interactions are not effectively equilibrated by spin diffusion sufficiently rapidly. The variation of the short- and long-time decay constants with temperature is similar, suggesting that they do not represent very different motional modes, but that they are associated with unequilibrated spin dynamics. The temperature dependencies of the longer [1]H $T_{1\rho}$ data for samples of IRMOF-3 (for samples with a ^{14}N natural abundance of 99.6% and with the nitrogen enriched in ^{15}N) are shown in Fig. 12.

The [1]H $T_{1\rho}$ data for both the natural-abundance ^{14}N IRMOF-3 and the ^{15}N-enriched IRMOF-3 in Fig. 12 show two maxima in the relaxation rate, $1/T_{1\rho}$, occurring at the same temperature for each compound, suggesting that the quadrupolar mechanism that operates in the T_1 measurements does not affect the magnetization in the rotating frame. The resulting relaxation rate can be treated as a sum of rates for two different processes:

$$\frac{1}{T_{1\rho}} = \frac{1}{T_{1\rho a}} + \frac{1}{T_{1\rho b}} \tag{1}$$

Proton spin–lattice relaxation in the rotating frame is induced by fluctuating dipolar couplings resulting from molecular motion. Each individual $T_{1\rho}$ process can be described by Eq. (2) from Look and Lowe [46].
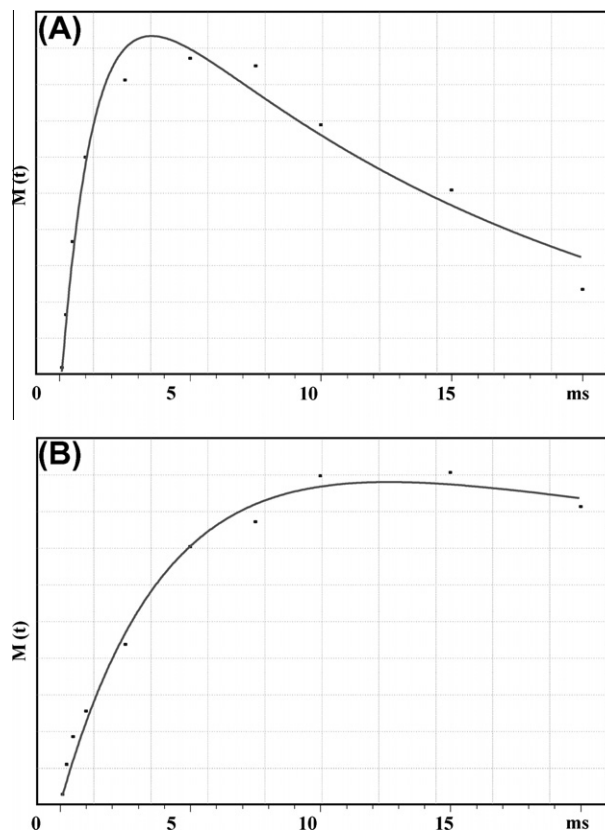

Fig. 9. [13]C CP/MAS variable-contact data (magnetization plotted in arbitrary units) of the carboxyl resonance in a sample of IRMOF-3 containing ^{14}N at natural abundance (A) and of a sample highly enriched in [15]N (B). The smooth line in each is a fit of Mehring's variable-contact model (see text).

$$\frac{1}{T_{1\rho}} = C \left\{ \frac{3}{2} \frac{\tau_c}{1 + \omega_1^2 \tau_c^2} + \frac{5}{2} \frac{\tau_c}{1 + \omega^2 \tau_c^2} + \frac{\tau_c}{1 + 4\omega^2 \tau_c^2} \right\} \tag{2}$$

where C is a constant with units of s^{-2} that represents the magnitude of the dipolar interaction; τ_c is the correlation time; and ω_1 is the amplitude of the spin-lock field, expressed as an angular frequency. The correlation time is assumed to be thermally activated and to follow an Arrhenius-type behavior:

$$\tau_c(T) = \tau_0 \exp \left[\frac{E_a}{RT} \right] \tag{3}$$

Activation energies, E_a, of 1.8(±0.6) and 5.2(±0.4) kcal/mol for the two processes are extracted from the simulation of the [1]H $T_{1\rho}$ data as shown in Fig. 12.

With the results obtained from the [1]H $T_{1\rho}$ data for the two samples of IRMOF-3 we turned our attention to the T_1 data shown in Fig. 4, plotted as the negative of the logarithm of the proton spin–lattice relaxation rate, $1/T_{1approx}$, as a function of the inverse temperature. The temperature dependence of the relaxation rate in each sample can be modeled by assuming that it is the result of (1) two thermally activated processes and (2) a temperature-independent contribution that dominates at low temperature, presumably due to the presence of quadrupolar ^{14}N atoms. The resulting relaxation rate was treated as a sum:

$$\frac{1}{T_1} = \frac{1}{T_{1,motional}} + \frac{1}{T_{1,N14}} \tag{4}$$

The $T_{1,motional}$ contribution was dominated by random modulation of proton–proton dipolar couplings, according to the equation [47,48]
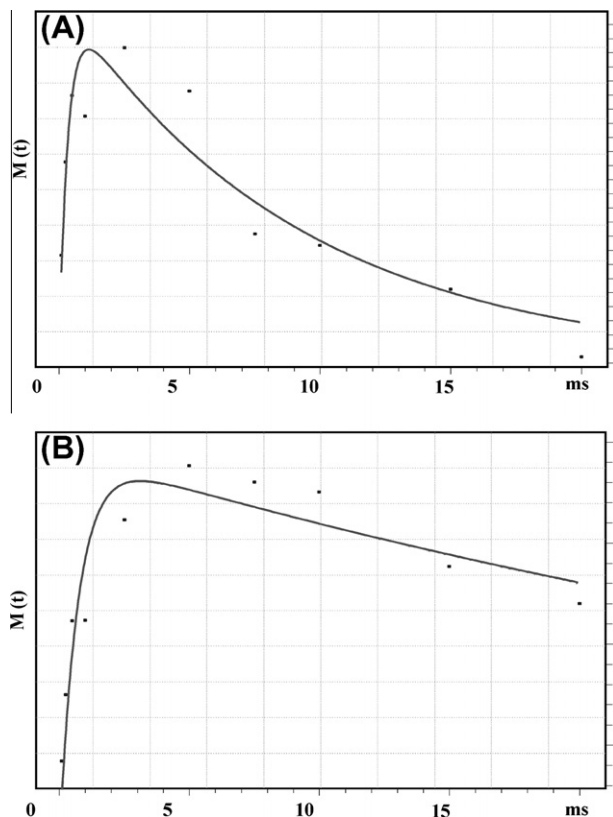
Fig. 10. ^{13}C CP/MAS variable-contact data (magnetization plotted in arbitrary units) for carbon 2 (aromatic NH$_2$-bearing carbon; see Fig. 1B) resonance in a sample containing ^{14}N at natural abundance (A) and of a sample highly enriched in ^{15}N (B). The smooth line in each is a fit to Mehring's variable-contact model (see text).

$$\frac{1}{T_1} = C\left[\frac{\tau_c}{1+\omega^2\tau_c^2} + \frac{4\tau_c}{1+4\omega^2\tau_c^2}\right] \qquad (5)$$

where C represents the magnitude of the dipolar interaction; τ_c is the correlation time; and ω is the Larmor frequency of the proton. A simulation of the temperature dependence of the spin–lattice relaxation data indicated a motional process with an energy barrier of 5.0($\pm$0.2) kcal/mol.

A comparison of the dynamics and activation parameters for IR-MOF-1 (MOF-5), IRMOF-2 and IRMOF-3 is very instructive. The 7.3 kcal/mol barrier to rotation reported for the bromo-*p*-phenylene moiety in IRMOF-2 [19] is 4.0 kcal/mol smaller than that reported for the unsubstituted phenylene in IRMOF-1 [18], which has a barrier of 11.3 kcal/mol. An additional decrease in activation energy of ca. 2.3 kcal/mol for amino-substituted IRMOF-3 highlights the effect of ring substituents, which may be analyzed in terms of electronic and/or steric effects. Of particular note for IR-MOF-2 is the X-ray diffraction data indicating that the bromo-*p*-phenylene rotor appears to be undergoing a "large angle libration in a flat-bottomed potential" with the "bromine atom librat(ing) more than the carbon atom to which it is attached" [19]. This observation appears to be the result of a steric destabilization of the ground-state structure by the relatively large bromine substituent in IRMOF-2, which causes the phenylene to rotate away from coplanarity and thus lose conjugation with the adjacent carboxylate. Some of the high-level calculations reported in the same article indicate that there are two energy minima linked by a shallow maximum that occurs when the ring is coplanar to the zinc oxide cluster carboxylates. It is interesting that the lower barrier for rotation in the case of IRMOF-2 relative to that in IRMOF-1 is due to destabilization of the ground state, instead of being the result of
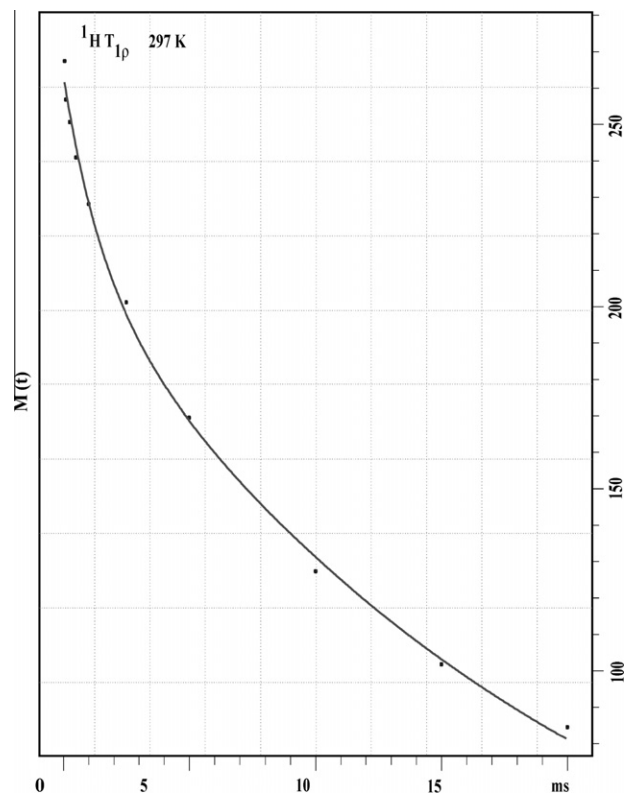

Fig. 11. ^{1}H spin–lattice relaxation data in the rotating frame ($T_{1\rho}$) for a sample of IRMOF-3 containing ^{14}N at natural abundance plotted in arbitrary units. The temperature was 297 K.
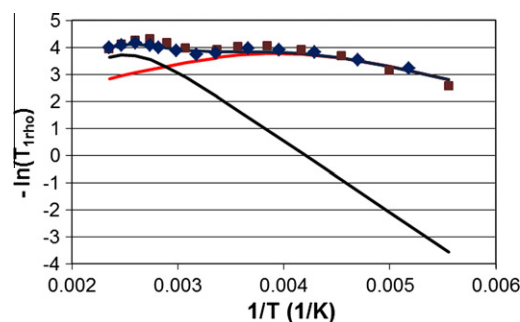

Fig. 12. The negative of the logarithm of $T_{1\rho}$ versus the inverse of the absolute temperature for IRMOF-3 containing ^{14}N at natural abundance. The experimental points are compared to a simulation, as described in the text ($\blacklozenge$ – enriched with ^{15}N; $\blacksquare$ – at natural abundance, 99.6% ^{14}N). The lines show the predicted temperature dependence of the two contributions to the relaxation.

a lower transition state. Considering that the van der Waals volume [49] of NH$_2$ (10.54 cm^3/mol) in IRMOF-3 is close to that of Br (14.40 cm^3/mol) in IRMOF-2, one may expect steric effects to be qualitatively similar. However, the relaxation of IRMOF-3 reveals significantly more complex dynamics.

Much of the discussion of molecular motions in the literature is cast in terms of an attempt or jump frequency (rate) rather than a correlation time. This attempt rate can be obtained by the inversion of Eq. (3) and is used below for comparison with previous studies.

The ^{1}H $T_{1\rho}$ data in Fig. 12 are consistent with a low-energy motion that has an activation energy of 1.2–1.8 kcal/mol, occurring prior to the onset of aromatic-ring flipping, which has a barrier of 5.0($\pm$0.2) kcal/mol. Considering that the low barrier process

may be associated with libration of the ring, we analyzed whether its pre-exponential factor would match the pre-exponential factor for the twofold flipping process [18,50], recognizing that they should have the same attempt frequency [51]. From a correlation time of 2.4×10^{-6} s derived from the ^1H $T_{1\rho}$ data at 260 K, one can determine a pre-exponential factor of ca. $1.3 \times 10^7 \, s^{-1}$ for the low barrier process. A similar analysis for the ring flipping motion reveals that a correlation time of 7.9×10^{-7} s at 365 K is associated with a pre-exponential factor of $1.19 \times 10^9 \, s^{-1}$ [52]. The difference of two orders of magnitude between the two processes indicates that they do not originate from elementary motions within the same potential energy well.

With the results from the ^1H $T_{1\rho}$ data as a guideline, we analyzed the ^1H T_1 data in Fig. 4. We note that thermal limitations of the NMR probe used in this study prevented determination of the temperature at which the maximal rate for ^1H spin–lattice relaxation occurs. However, the simulation of the data in Fig. 4 also yields an activation energy of 5.0(±0.2) kcal/mol. The similarity of this value suggests that the motion is the same one responsible for the higher-temperature ^1H $T_{1\rho}$ minimum around 365 K. A complete simulation of the ^1H spin–lattice relaxation data in Fig. 4 for either sample requires the inclusion of a temperature-independent mechanism at the lower temperatures. In the sample containing ^{14}N at natural abundance, another thermally activated motion ($E_a \sim 1.25$ kcal/mol) appears at lower temperature. While this process could be related to the libration observed to affect $T_{1\rho}$ with an activation energy of 1.8 kcal/mol, this mechanism is not effective for the sample enriched in ^{15}N, suggesting that the process is mediated by the quadrupolar nucleus.

The barrier of the low-energy process is of similar magnitude to the barrier usually observed for simple methyl group rotation in solids [53]. Low-energy processes in aromatic amines may include nitrogen inversion and amine rotation. While the two processes are correlated [54], only the latter is expected to provide an efficient relaxation mechanism. The barrier for rotation in aniline itself is ca. 4 kcal/mol [54,55], but it is known to be highly sensitive to steric and electronic effects. However, a pre-exponential factor of $1.3 \times 10^7 \, s^{-1}$ for this process is much smaller than those typically associated with inversion and torsional modes, which are $>10^{12} \, s^{-1}$. We speculate that the small pre-exponential factor deduced in this study is an indication that the rate-limiting step for rotation may be determined by the rupture of a hydrogen bond between the NH_2 group and the neighboring carboxylate. The dynamic model that we envision at low temperatures involves a thermally activated cleavage of the hydrogen bond as a rate-limiting step for NH_2 rotation. Higher thermal energies would lead to faster NH_2 rotation accompanied by a faster aromatic ring flipping, with the latter becoming the dominant relaxation mechanism. With respect to the lack of a low-energy process in ^1H T_1 experiments with the ^{15}N-labeled sample, one should note that a maximum possible frequency of 13 MHz, given by the pre-exponential factor, is far from the Larmor frequency of the ^1H spins at 300 MHz. This indicates that NH_2 rotation in IRMOF-3 can only be an effective spin–lattice relaxation mechanism in low field experiments. We intend to test this hypothesis in due time.

4. Conclusions

The framework motions in IRMOF-3 have been investigated with ^1H NMR relaxation measurements. These results indicate a libration of the amino group with an activation energy of ca. 1.8(±0.6) kcal/mol and a flip motion of the amino phenylene moiety with an activation energy of 5.0(±0.2) kcal/mol. Both the libration of the amino group and the aromatic-ring flip occur at frequencies that provide an effective relaxation mechanism for

the 99.6% natural abundance quadrupolar ^{14}N in the amino group. Dipolar coupling of the ^{14}N to adjacent spin-½ nuclei (both ^1H and ^{13}C) occurs not only in the static sample but also in the MAS experiments at the magnetic field of 7 T used in this study. As a result, the spin dynamics and the cross-polarization dynamics are affected. In the MAS experiments, isotopic replacement of the natural abundance ^{14}N with ^{15}N significantly improves resolution in the ^1H, ^{13}C and ^{15}N spectra.

References

[1] H. Li, M. Eddaoudi, T.L. Groy, O.M. Yaghi, J. Am. Chem. Soc. 120 (1998) 8571–8572.
[2] H. Li, M. Eddaoudi, M. O'Keeffe, O.M. Yaghi, Nature 402 (1999) 276–279.
[3] C. Janiak, J.K. Vieth, New J. Chem. 34 (2010) 2366–2388.
[4] R. Banerjee, H. Furukawa, D. Britt, C. Knobler, M. O'Keeffe, O.M. Yaghi, J. Am. Chem. Soc. 131 (2009) 3875–3877.
[5] S. Surblé, C. Serre, C. Mellot-Draznicks, F. Millange, G. Férey, Chem. Commun. (2006) 284–286.
[6] C.-D. Wu, L. Ma, W. Lin, Inorg. Chem. 47 (2008) 11446–11448.
[7] M. Eddaoudi, J. Kim, N. Rosi, D. Vodak, J. Wachter, M. O'Keeffe, O.M. Yaghi, Science 295 (2002) 469–472.
[8] J.L.C. Rowsell, O.M. Yaghi, Microporous Mesoporous Mater. 73 (2004) 3–14.
[9] Z. Wang, S.M. Cohen, J. Am. Chem. Soc. 129 (2007) 12368–12369.
[10] Z. Wang, S.M. Cohen, Chem. Soc. Rev. 38 (2009) 1315–1329.
[11] D. Britt, C. Lee, F.J. Uribe-Romo, H. Furukawa, O.M. Yaghi, Inorg. Chem. 49 (2010) 6387–6389.
[12] M.J. Ingleson, J.P. Barrio, J-B. Guilbaud, Y.Z. Khimyak, M.J. Rosseinsky, Chem. Commun. (2008) 2680–2682.
[13] C.J. Doonan, W. Morris, H. Furukawa, O.M. Yaghi, J. Am. Chem. Soc. 131 (2009) 9492–9493.
[14] K.K. Tanabe, S.M. Cohen, Angew. Chem. 121 (2009) 7560–7563.
[15] W. Morris, B. Leung, H. Furukawa, O.K. Yaghi, N. He, H. Hayashi, Y. Houndonougbo, M. Asta, B.B. Laird, O.M. Yaghi, J. Am. Chem. Soc. 132 (2010) 11006–11008.
[16] S. Amirjalayer, M. Tafipolsky, R. Schmid, Angew. Chem. Int. Ed. 46 (2007) 463–466.
[17] J. Gonzalez, R. Nandini Devi, D.P. Tunstall, P.A. Cox, Paul A. Wright, Microporous Mesoporous Mater. 84 (2005) 97–104.
[18] S.L. Gould, D. Tranchemontagne, O.M. Yaghi, M.A. Garcia-Garibay, J. Am. Chem. Soc. 130 (2008) 3246–3247.
[19] E.B. Winston, P.J. Lowell, J. Vacek, J. Chocholoušová, J. Michl, J.C. Price, Phys. Chem. Chem. Phys. 10 (2008) 5188–5191.
[20] S.D. Karlen, M.A. Garcia-Garibay, Topics Curr. Chem. 262 (2005) 179–227.
[21] W. Zhou, H. Wu, T. Yildirim, J.R. Simpson, A.R. Hight Walker, Phys. Rev. B 78 (2008) 054114.
[22] B.L. Huang, A.J.H. McGaughley, M. Kaviany, Int. J. Heat Mass Transfer 50 (2007) 393–404.
[23] J. Schaefer, E.O. Stejskal, J. Am. Chem. Soc. 98 (1976) 1031–1032.
[24] J.L.C. Roswell, O.M. Yaghi, J. Am. Chem. Soc. 128 (2006) 1304–1315.
[25] R.K. Harris, E.D. Becker, S.M. Cabal De Menezes, R. Goodfellow, P. Granger, Pure Appl. Chem. 73 (2001) 1795–1818.
[26] T.C. Farrar, E.D. Becker, Pulse and Fourier Transform NMR, Introduction to Theory and Methods, Academic Press, New York, 1971.
[27] L.M. Ryan, R.E. Taylor, A.J. Paff, B.C. Gerstein, J. Chem. Phys. 72 (1980) 508–515.
[28] D.P. Burum, D.G. Cory, K.K. Gleason, D. Levy, A. Bielecki, J. Magn. Reson. Series A 104 (1993) 347–352.
[29] R.K. Harris, E.D. Becker, S.M. Cabal De Menezes, P. Granger, R.E. Hoffman, K.W. Zilm, Solid State NMR 33 (2008) 41–56.
[30] L.J. Burnett, B.H. Muller, Chem. Phys. Lett. 18 (1973) 553–556.
[31] R.C.T. Slade, T.K. Halstead, P. McGeehin, Solid State Commun. 31 (1979) 343–346.
[32] G. Ślósarek, S. Idziak, N. Piślewski, J. Stankowski, Phys. Status Solidi B 110 (1982) 233–238.
[33] A. Kozak, Z. Pajak, N. Piślewski, Chem. Phys. Lett. 74 (1980) 173–175.
[34] P.A. Beckman, S. Bai, C. Dybowski, Phys. Rev. B 71 (2005) 012410.
[35] T.K. Pratum, M.P. Klein, J. Magn. Reson. 81 (1989) 350–370.
[36] T. Giavani, H. Bildsøe, J. Skibsted, H.J. Jakobsen, J. Magn. Reson. 166 (2004) 262–272.
[37] J.-R. Suhr, C.-J. Yoon, S.-G. Ro, Y.-S. Choi, Bull. Korean Chem. Soc. 8 (1987) 230–232.
[38] M.D. Harmony, P.A. Baron, J. Mol. Struct. 38 (1977) 1–8.
[39] W.P. Rothwell, J.S. Waugh, J. Chem. Phys. 74 (1981) 2721–2732.

[40] E. Pretsch, J. Seibl, T. Clerc, K. Biemann, Tables of Spectral Data for Structure Determination of Organic Compounds, second ed., Springer-Verlag, Berlin, 1989. pp. C120–C125.

[41] M.E. Stoll, R.W. Vaughan, R.B. Saillant, T. Cole, J. Chem. Phys. 61 (1974) 2896–2899.

[42] S.J. Opella, M.H. Frey, T.A. Cross, J. Am. Chem. Soc. 101 (1979) 5856–5857.

[43] N. Zumbulyadis, P.M. Henrichs, R.H. Young, J. Chem. Phys. 75 (1981) 1603–1611.

[44] A.C. Olivieri, J. Magn. Reson. 81 (1989) 201–205.

[45] M. Mehring, High resolution NMR spectroscopy in solids, in: P. Diehl, E. Fluck, R. Kosfeld (Eds.), NMR 11: Basic Principles and Progress, Springer-Verlag, Berlin, 1976, pp. 135–153.

[46] D.C. Look, I. Lowe, J. Chem. Phys. 44 (1966) 3441–3452.

[47] E.R. Andrew, W.S. Hinshaw, M.G. Hutchins, R.O.I. Sjöblom, Mol. Phys. 31 (1976) 1479–1488.

[48] R. Kubo, K. Tomita, J. Phys. Soc. Jpn. 9 (1954) 888–919.

[49] A. Bondi, J. Phys. Chem. 68 (1964) 441–451.

[50] S.D. Karlen, H. Reyes, R.E. Taylor, S.I. Khan, M.F. Hawthorne, M.A. Garcia-Garibay, Proc. Natl Acad. Sci. USA 107 (2010) 14973–14977.

[51] G.S. Kottas, L.I. Clarke, D. Horinek, J. Michl, Chem. Rev. 105 (2005) 1281–1376.

[52] The pre-exponential factors for ring flip in IRMOF-1 and IRMOF-2 are $1.6 \times 10^{12}\ s^{-1}$ and 3.5–$6.5 \times 10^{11}\ s^{-1}$, respectively, from references 16 and 17.

[53] P.A. Beckmann, C. Dybowski, E.J. Gaffney, C.W. Mallory, F.B. Mallory, J. Phys. Chem. A 105 (2001) 7350–7355.

[54] M.A. Palafox, M. Gill, N.J. Nunez, V.K. Rastogi, L. Mittal, R. Sharma, Int. J. Quantum. Chem. 103 (2005) 394–421.

[55] J.C. Jiang, C.E. Lim, J. Mol. Struct. (Theochem) 392 (1997) 181–191.